Numerical Study of Turbulent Flow Aerodynamics Around a Multi-Element Airfoil

Elhassen Omer [1*] 🆔, Ali Alkharboushi [1] 🆔, Zainab Ahmed [2] 🆔

[1] Mechanical Engineering Department, Faculty of Engineering, University of Zawia, Zawia, Libya

[2] Aeronautical Engineering Department, Faculty of Engineering, University of Tripoli, Tripoli, Libya

*Corresponding author email: e.amr@zu.edu.ly

ABSTRACT

Multi-element airfoils are high-lift devices and provide improved aerodynamic characteristics, which are beneficial for several applications. The performance of high lift devices was investigated numerically by adapting the 2D viscous, steady, pressure model equations together with the SST k-ω turbulence model. Simulations were performed using ANSYS Fluent 24 for the NHLP2D airfoil with a leading edge slat and trailing edge flap. The flow is considered at a Reynolds number of 1.6×10^5 and varying angles of attack from 0 to 28 deg. The parameters that describe the positioning of the slat and flap were tested variables. These variables include deflection angles, gaps, and overlaps. The lift and drag coefficients are evaluated for various configurations. The results reveal that slats increase the maximum lift on the wing and delay stall, increasing the maximum angle of attack. However, they reduce the lift. In contrast, the flaps increase the overall high-lift configuration airfoil camber, thereby increasing lift. It was found that for the tested slats and flaps locations, slats with a 2.6% gap, -1.5% overlap and 30° deflection, and flap with a 1.3% gap, 5.3% overlap and 30° deflection was the one with the most favorable performance, generating a Cl_{max} of 3.81 and Cd of 0.158.

Keywords: High lift devices, Multi-element airfoil, Lift coefficient, Drag coefficient, CFD.

دراسة الديناميكيا الهوائية للتدفق المضطرب حول الجنيح متعدد الأجزاء

الحسن عمرو[1]، علي الخربوشي[1] ، زينب أحمد[2]

[1] قسم الهندسة الميكانيكية والصناعية، كلية الهندسة، جامعة الزاوية، الزاوية، ليبيا.

[2] قسم هندسة الطيران، كلية الهندسة، جامعة طرابلس، طرابلس، ليبيا.

ملخـــــص البحـــــث

تعتبر الجنيحات متعددة الأجزاء أجهزة لزيادة وتوفر خصائص ديناميكية هوائية محسنة مفيدة للعديد من التطبيقات الهندسية.
تمت محاكاة للتدفق المضطرب فوق الجنيح NHLP2D مع شريحة الحافة الأمامية ورفرف الحافة الخلفية باستخدام
ANSYS Fluent 24. تم تطبيق معادلات نموذج الضغط اللزج والثابت ثنائي الأبعاد مع نموذج الاضطراب SST
k-ω على هذه المحاكاة العددية. وأجريت الدراسة عند رقم رينولدز 1.6×10^5 وزوايا هجوم من 0 إلى 28 درجة. وفي

هذا البحث تم دراسة تأثير المتغيرات التي تصف موضع عناصر الجنيح، وتتضمن زوايا الانحراف والفجوات والتداخلات. حيث يتم حساب معاملات الرفع والسحب لمختلف التكوينات الممكنة. وأظهرت النتائج أن خصائص الديناميكية الهوائية قد تم رفعها وكشفت النتائج أن إضافة الشرائح الأمامية تزيد من الحد الأقصى للرفع على الجناح وتأخير المماطلة مما يزيد من الزاوية القصوى للهجوم، وإضافة الرفارف تزيد من الحدبة الجنيحية الكاملة لتكوين الرفع العالي. ولقد وجد أنه بالنسبة لمواقع الشرائح والرفارف التي تم اختبارها، فإن الشرائح ذات فجوة 2.6%، وتداخل −1.5% وانحراف 30 درجة، والرفرف ذو فجوة 1.3%، وتداخل 5.3%، وانحراف 30 درجة هي الأكثر ملاءمة، والتي تؤدي إلى توليد C_{lmax} بقيمة 3.81 و C_d بقيمة 0.158.

الكلمات الدالة: أجهزة الرفع العالي، الجنيح متعدد العناصر، معامل الرفع، معامل السحب، CFD.

1. Introduction

The High-lift capability of an aircraft plays an important role in the design of military and commercial aircrafts. Improved high lift performance leads to increased range and payload as well as decreased landing speed and field length requirements. Typical high-lift systems, often consisting of a basic wing with a leading-edge slat and trailing-edge flap elements, are highly efficient aerodynamically, but at the expense of complex structure, design and expensive maintenance costs. Slats are aerodynamic surfaces on a fixed wing leading edge, which allow the air to flow more smoothly over the upper surface at higher angles of attack. A higher coefficient of lift is produced as a result of angle of attack and speed, so by deploying slats, an aircraft can fly at slower speeds, or take off and land in shorter distances. They are usually used while landing or performing manoeuvres which take the aircraft close to stall, but are usually retracted in normal flight to minimize drag. Flaps are a movable portion of the rear wing that can be lowered into the airflow to reshape and increase the wing chord and area to produce extra lift. They shorten take-off and landing distances by lowering the stall speed and increasing drag. Extending flaps increases drag, which can be beneficial during approach and landing, because it slows the aircraft [1, 2].

Multi-element airfoils have been studied extensively, since these airfoils have been used to improve the aerodynamic performance, which can be used in various engineering applications such as airplane wings, wind turbines, etc.   The flow around the three-element aerodynamic airfoil 30P30N was studied experimentally [3-5], for different flight configurations in the range of Reynolds numbers from 1.6×10^5 to 1.1×10^6 and the angles of attack from 0 ° to 12°. As is the case for the majority of high-lift systems, the leading edge slat and trailing edge flap are deployed to improve lift. The slat extends the lift curve to a larger stall angle, while the flap increases lift, shifting the curve up. Numerically, the turbulent flow around the three-element airfoils, [6-12] was investigated using the commercially available software ANSYS Fluent to manage the structure of the flow around the multi-element airfoils.   The Reynolds number is in the range of $(1.6-4.7) \times 10^6$, at angles of attack in the range of   0° - 30°.   Their results report that the lift coefficient, drag coefficient, and lift-to-drag ratio produced with the addition of flaps and slats showed significant differences compared to the plain wing. These variations can be used for certain conditions, such as take-off, cruising, and landing. The vorticity magnitude and vortex produced by the addition of a high lift device showed a significant improvement in aerodynamic characteristics compared to plain wings. The panel method using XFOIL and XFLR5 programs was used [13-15], for investigating lift and drag phenomena of the flow field over different airfoils, such as 30P30N, GA (W)-1, RAF16, and NLR 7301 airfoils. The results show a delayed stall because of the slat at the leading edge, which helped in generating a higher lift.   At higher angles of attack, the coefficient of lift on the flap reduced, but increased on the slat, whereas the coefficient of drag   remains steady up to 10° angle

of attack and then decreases at higher angles of attack. When both the flap and slat elements have been used, the highest lift and drag coefficients reported are 3.67 and 0.36. The aerodynamic characteristics of airfoils with and without flaps were studied numerically, [16], through Fluent and XFRL5, the Reynolds number was fixed, and the angle of attack varied. The objective of their study was to verify which airfoil and its availability would be more aerodynamically efficient. Also, which numerical method is more feasible for the realization of two-dimensional simulations in incompressible aerodynamics. From the results presented, the simulations showed that when analyzed only the airfoils without flap, the asymmetric one has a superior lift coefficient and drag coefficients similar to those presented by the symmetrical profile. When flap profiles were evaluated, it was verified that the asymmetric in the same way as when the flaps had better C_L/C_D ratios than the symmetrical airfoils. Finally, it was observed that Fluent software has greater robustness with aerodynamic analysis when compared to XFRL5. However, it requires a higher computational cost.

In this work, a numerical simulation of the flow around multi-element airfoils was studied, aiming to investigate the optimum location and orientation of the high lift devices. The key parameters involved in the multi-element airfoils design are deflection or orientation angle, overlap and gap distance, and their variation will enable us to observe their influence on the overall performance of the airfoil configurations required for the intended application.

2. Methodology

In the present study, the high fidelity ANSYS Fluent was used to solve Reynolds Averaged Navier Stokes equations (RANS), describing the flow over multi-element airfoil to compute the aerodynamic characteristics of aircraft in high-lift configurations.

2.1 Mathematical Modelling

In the present study, ANSYS Fluent was used to solve Reynolds Averaged Navier Stokes equations (RANS), these equations are based on the fundamental concepts of conservation of mass, energy and momentum. It was assumed that the flow is steady and incompressible. Thus, the governing equations are [17]:

$$\frac{\partial}{\partial x_i}(\rho u_i) = 0 \tag{1}$$

$$\frac{\partial}{\partial x_j}(\rho u_j u_i) = -\frac{\partial P}{\partial x_i} + \frac{\partial}{\partial x_j}\left[\mu\left(\frac{\partial u_i}{\partial x_j}+\frac{\partial u_j}{\partial x_i}\right)\right] + \frac{\partial}{\partial x_j}(-\rho\overline{u_i'u_j'}) \tag{2}$$

The normal Reynolds stress, which is combined by the Boussinesq relationship and the eddy viscosity, is given by

$$-\rho\overline{u_i'u_j'} = \mu_t\left(\frac{\partial u_i}{\partial x_j}+\frac{\partial u_j}{\partial x_i}\right) \tag{3}$$

Where:
p   pressure, (Pa).
u, u'   velocity component and velocity fluctuations, (m/s).
x   spatial coordinates, (m).
ρ   density, (kg/m³).
μ   dynamic viscosity, (kg/ms).
μ_t turbulent viscosity, (kg/ms).

The shear stress transport (SST) k −ω model turbulent model was chosen in most aerodynamics applications. The model is a two-equation eddy-viscosity closure, [18] :

$$\frac{\partial \rho k}{\partial t} + \frac{\partial \rho u_j k}{\partial x_j} = P - \beta^* \rho \omega k + \frac{\partial}{\partial x_j}\left[(\mu + \sigma_k \mu_t)\frac{\partial k}{\partial x_j}\right] \tag{4}$$

$$\frac{\partial \rho \omega}{\partial t} + \frac{\partial \rho u_j \omega}{\partial x_j} = \frac{\alpha}{v_t} P - \beta \rho \omega^2 + \frac{\partial}{\partial x_j}\left[(\mu + \sigma_\omega \mu_t)\frac{\partial k}{\partial x_j}\right] + 2(1 - F_1)\frac{\rho \sigma \omega^2}{\omega}\frac{\partial k}{\partial x_j}\frac{\partial \omega}{\partial x_j} \tag{5}$$

The $k - \omega$ SST model in ANSYS expresses the turbulent viscosity as:

$$\mu_t = \frac{\rho a_1 k}{max[a_1 \omega, SF_2]'} \tag{6}$$

Where:

k   Turbulent kinetic energy, (J kg^{-1}).

ω   Specific dissipation rate, (m^2/s).

$$S = \sqrt{2 S_{ij} S_{ji}} \tag{7}$$

The expression for the mean strain rate tensor Sij and the expression for the production term P are :

$$S_{ij} = \frac{1}{2}\left(\frac{\partial \overline{u_i}}{\partial x_j} + \frac{\partial \overline{u_j}}{\partial x_i}\right) \tag{8}$$

$$P = min\left[\tau_{ij}\frac{\partial u_i}{\partial x_j}, 10\beta^* \rho \omega k\right] \tag{9}$$

ANSYS Fluent calculates F1 and F2 using the expressions below:

$$F_1 = \tanh\left(min\left[max\left[\frac{\sqrt{k}}{\beta^* \omega d}, \frac{500v}{d^2 \omega}\right], \frac{4\rho \sigma_{\omega 2} k}{CD_{k\omega} d^2}\right]^4\right) \tag{10}$$

$$F_2 = \tanh\left(max\left[2\frac{\sqrt{k}}{\beta^* \omega d}, \frac{500v}{d^2 \omega}\right]^2\right) \tag{11}$$

$$CD_{k\omega} = max\left[2\rho \sigma_{\omega 2}\frac{1}{\omega}\frac{\partial k}{\partial x_j}\frac{\partial \omega}{\partial x_j}, 10^{-10}\right] \tag{12}$$

The model constants and parameters used in the model [19]:

$\alpha_1 = \frac{5}{9}$ $\alpha_2 = 0.44$ $\sigma_{k1} = 0.85$ $\sigma_{\omega 1} = 0.500$ $\beta_1 = 0.075$

$\sigma_{k2} = 1.00$ $\sigma_{\omega 2} = 0.856$ β_2 0.0828 $\beta^* = 0.09$ $k = 0.41$ $\alpha_1 = 0.31$

2.2 Performance Characteristics

The model selected for examination is NHLP-2D, [20]. a two-dimensional supercritical airfoil with high-lift devices, which includes a 12.5%C leading edge slat and a 33%C single-slotted flap, where C is the chord length of the nested configuration. The aerodynamic performance of multi-element airfoil systems is highly dependent on deflection angles, overlap distance, and gap sizes between the elements.   The deflection angle of the main element was taken as zero. A positive deflection angle corresponded to a downward flap deflection. The location of the flaps was constrained by the overlap distance and gap size. The overlap is defined as the minimum distance between the leading/trailing edge of the main element and the associated trailing/leading edge of the considered high-lift device. For both the slat and the flap device, the origin of the overlap measurement is located at the leading/trailing edge of the main airfoil, resulting in positive and negative values of overlaps between the devices.   The gap is defined as the minimum distance of the gap between the trailing edge point of the forward element and the surface of the backwards element [21]. Figure 1 defines the deflection angles and indicates measurement of gaps and overlaps.
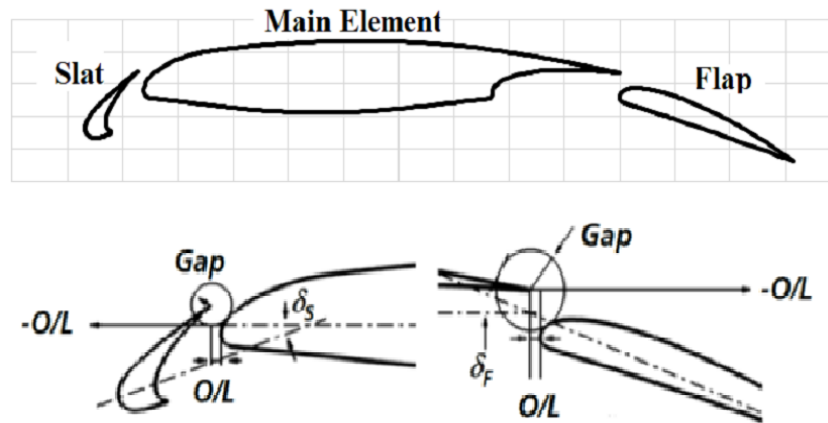
Figure 1. Definition of NHLP airfoil parameters gap, overlap (O/L) and deflection angle

The slat and flap optimum locations will be investigated. The flow conditions for this study are freestream Mach number Ma = 0:117 and Re = 2.7 x 10^5, and the angle of attack in the range of (0 - 28) degrees, In these simulations, the lift and drag coefficients were used as the performance evaluation parameters, and calculated using the induced forces of the flow as follows, [22]:

$$C_L = \frac{F_L}{0.5\rho u_\infty^2 \, C} \tag{13}$$

$$C_D = \frac{F_D}{0.5\rho u_\infty^2 \, C} \tag{14}$$

Where :

F_L Lift force, (N).
F_D Drag force, (N).
u_∞ Free stream velocity, (m/s).
C   Stowed chord length, (m).
ρ   Air density, (kg/m^3).

2.3 Numerical Methods

The numerical flow simulations are conducted with ANSYS FLUENT. The steady Reynolds-averaged Navier-Stokes equations (RANS) are solved by means of a pressure based solver. Turbulence modelling is performed by the shear stress transport SST $k - \omega$ turbulence model, and turbulence properties at the boundaries are set in order to provide a turbulence intensity of 0.5% at the front of the computational domain. The coupled algorithm is used over the regular segregated algorithms, since the coupled solver is more efficient and thus performs better than the standard algorithms. The second-order pressure scheme is employed for the pressure interpolation, and second-order upwind schemes are chosen for the spatial discretization of momentum, turbulent kinetic energy and specific dissipation rate. Moreover, a least squares cell-based formulation is used for the gradient calculation. C-type computational domain was chosen for simulations. The radius of the C part of the domain is 13 times the chord length, and the far field length downstream is 26C. This choice is based on the results of numerical and experimental investigation of Suvanjumrat, [23] to obtain the appropriate domain dimensions giving accurate results of lift and drag coefficients. An unstructured mesh was generated by specifying an edge mesh to all edges, then putting a triangular unstructured mesh onto the face. The domain and its meshing are shown in Figure 2.

The multi-element airfoil is located in the middle of the domain to ensure there are no reflecting influences from boundaries.
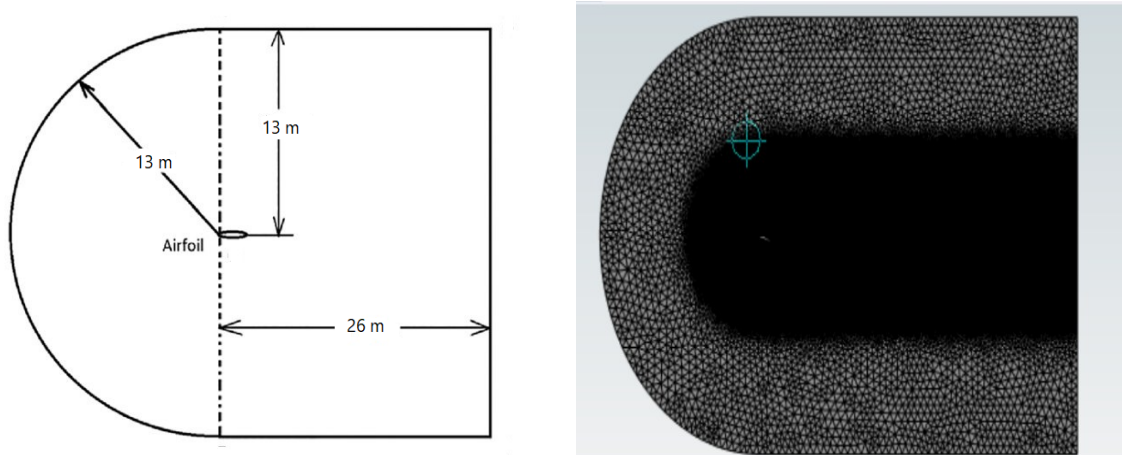

Figure 2. The computational domain dimensions and meshing

The region in the vicinity of the airfoil was denser as shown in Figure 3, and the distance of the first grid from the wall surface in the boundary layer is set to 1×10^{-5} m with the growth ratio of 1.15.   The total number of grids is almost 500,000. In addition to a no-slip wall boundary condition applied at the airfoil surface, pressure outlet and velocity inlet conditions were imposed at the computational domain boundaries.
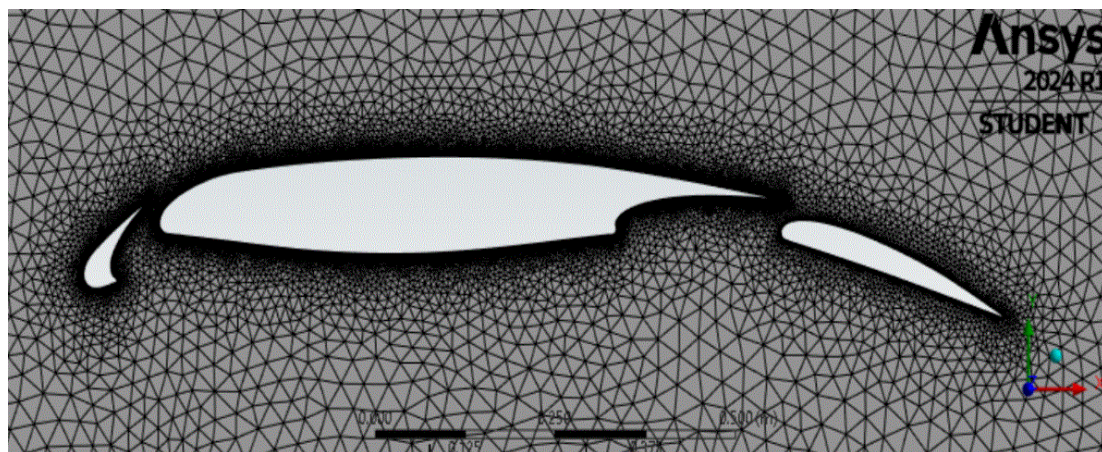
Figure 3. The computational mesh in the vicinity of the airfoil

3.   Grid Independence Testing and Code Validation

For more accurate results, more nodes are needed, and using more nodes will escalate the requisite computational time and computer memory. To obtain greater sensitivity to grid refinement in the results, many types of grids are applied, and the coefficients of lift for the multi-element airfoil with Re = 1×10^{6} at $\alpha = 15°$ are examined.   Meshing considerations are used when the difference between the lift coefficient and the previous meshing is approximately less than 1%. Another consideration is that the best use of $y+$ is below the value of 1. Also, the mesh quality measures, such as orthogonality quality and skewness, were as recommended by Fluent [24]. The mesh independence test results are given in

Table 1. According to the above considerations, the C mesh was chosen for further calculation in this study.

Table 1: Grid independence test and mesh quality parameters

Mesh	Number of Nodes	Cl	Orthogonal Quality	Average Skewness	y+
A	188944	2.26577	0.96046	5.88E-02	5.18941
B	311270	2.98812	0.9634	6.23E-02	3.04466
C	**430533**	**3.38937**	**0.96527**	**6.13E-02**	**0.60510**
D	718318	3.40841	0.96643	6.06E-02	0.05728

The multi-element airfoil results are compared with the experimental and OPENFOAM numerical results obtained by Sereez et. al, [25]; these comparisons are shown in Figure 4. There is a good agreement between the numerical results in the linear part of the Cl curve, indicating attached flow up to an angle of attack, α = 12°. At higher values of angle of attack, the Cl curve slope starts to decline, indicating increasing separation over the airfoil. The stall is at α = 22°, which is the same as obtained in the experimental and numerical results. Beyond the stall angle, there is a sharp drop was observed in the lift force coefficient, where the flow separation has reached full development.
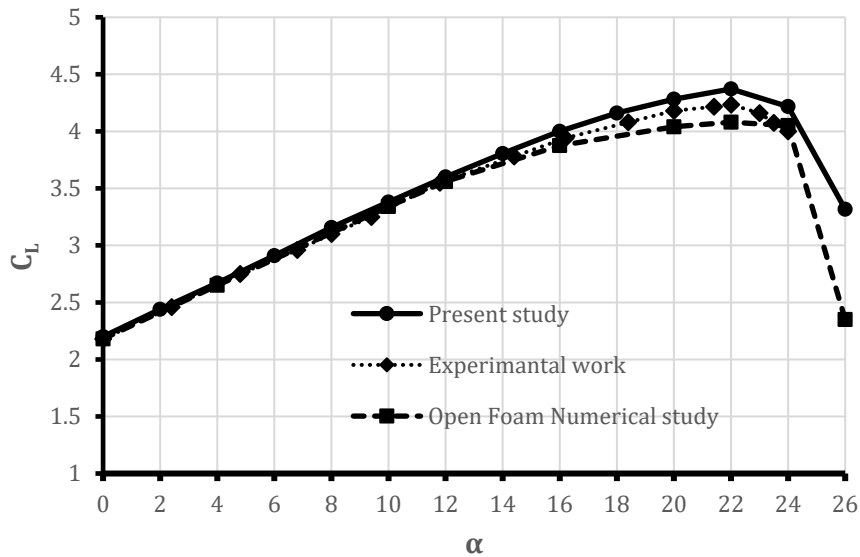

Figure 4. Validation of the current study and numerical and experimental results by [25].

4.   Results and Discussion

The investigation of the different location parameters on the performance of leading and trailing edge flaps is presented and analyzed.

4.1 Leading edge slap effects

For this portion of the study, the flap was set at 20° deflection with an overlapping of 5.3% and a gap of 1.3%. The flap position was fixed while the deflection slat angle, slat overhang and gap were varied.

i. Effect of deflection angle

Figure 5 shows the C_L value for each angle of attack of the airfoil with various deflection angles. As the leading-edge slat deflection increases, the lift coefficient generally increases due to enhanced airflow over the wing. The increase in C_L becomes more pronounced up to about 30° to 35°, where significant lift improvements are noted, especially at higher angles of attack. Figure 6 shows the obtained values of Cd, Drag increases with slat deflection. This is due to increased surface area and changes in airflow that lead to higher induced drag. While lift increases, the increase in drag can offset some of the benefits, particularly at higher deflection angles.
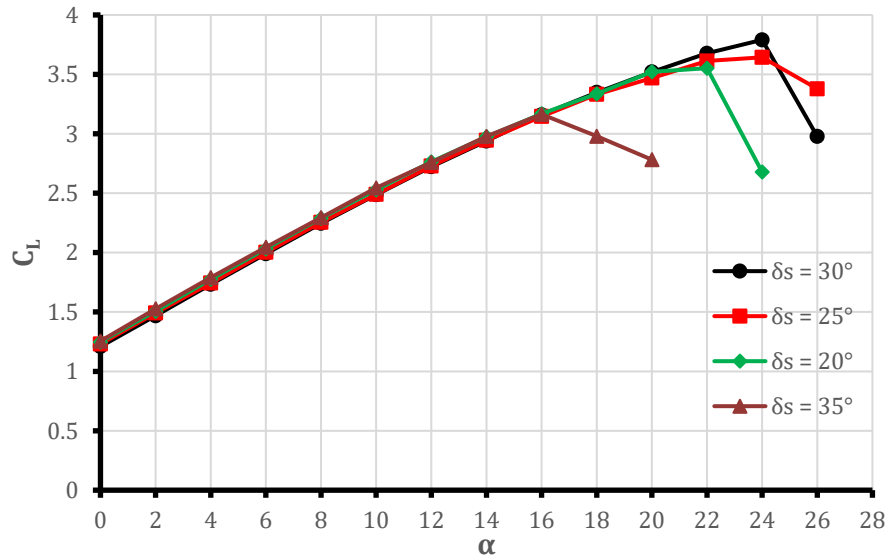
Figure 5. Lift coefficient for different deflection angles of the slat.
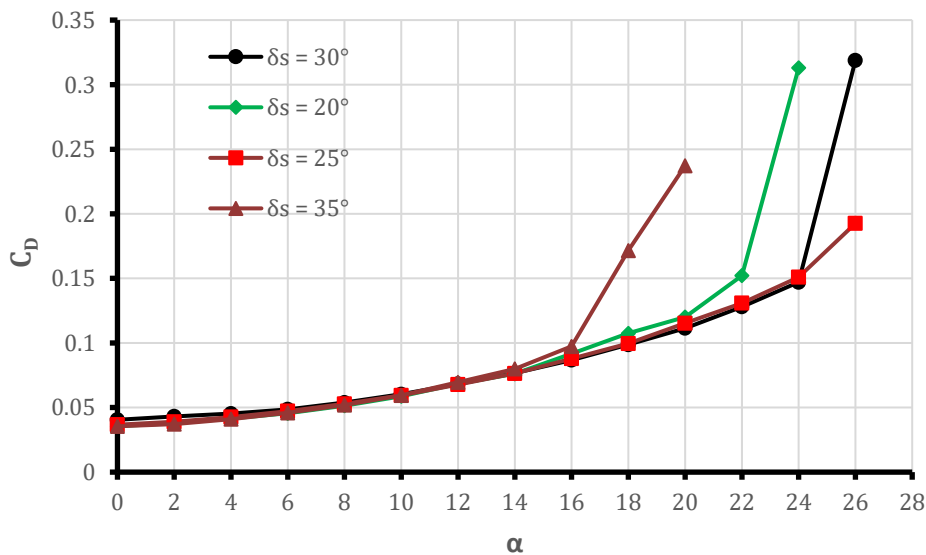
Figure 6. Drag coefficient for different deflection angles of the slat.

ii. Effect of gap

Figures 7 and 8 show the effect of gap on aerodynamic characteristics, that is, cl and cd of slat locations at different gaps. A smaller gap tends to maintain a better interaction between the slat and main wing, enhancing lift at low speeds and high angles of attack. Also, the smaller gap promotes smoother airflow, reducing the likelihood of flow separation and delaying stall. About the drag, it increases due to the presence of additional surfaces. As the gap value increases to 3.27%C the lift is adequate, but it could be slightly less efficient than the smaller gap. The larger gap may introduce some flow disruption, slightly increasing drag, but typically not as significantly as in larger gaps.

As the gap increased from 2.6%C to a larger gap value of 4.1%C, the flow separation is increased, particularly at higher angles of attack, resulting in a sharp decrease in the maximum-lift coefficient and higher stall risk. This larger gap can significantly increase drag due to greater flow separation and turbulence, adversely affecting the lift-to-drag ratio.
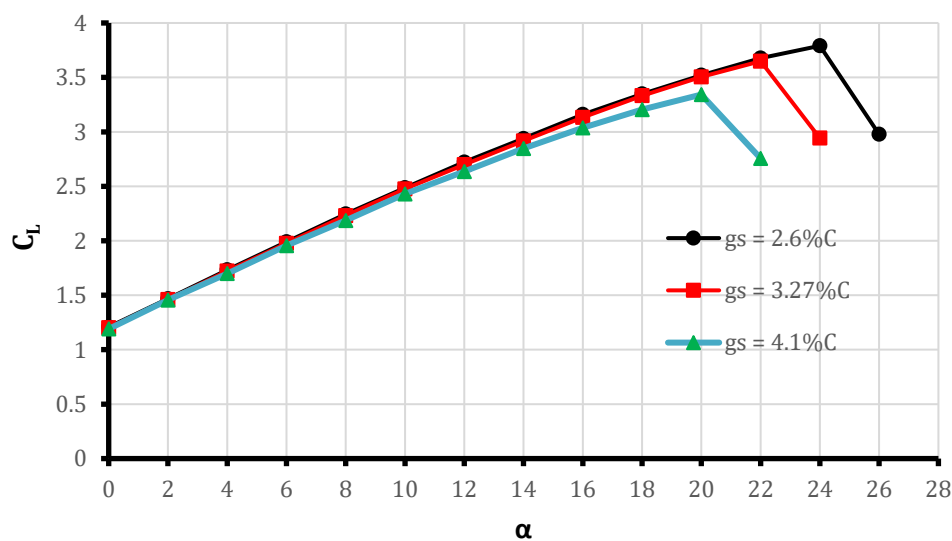

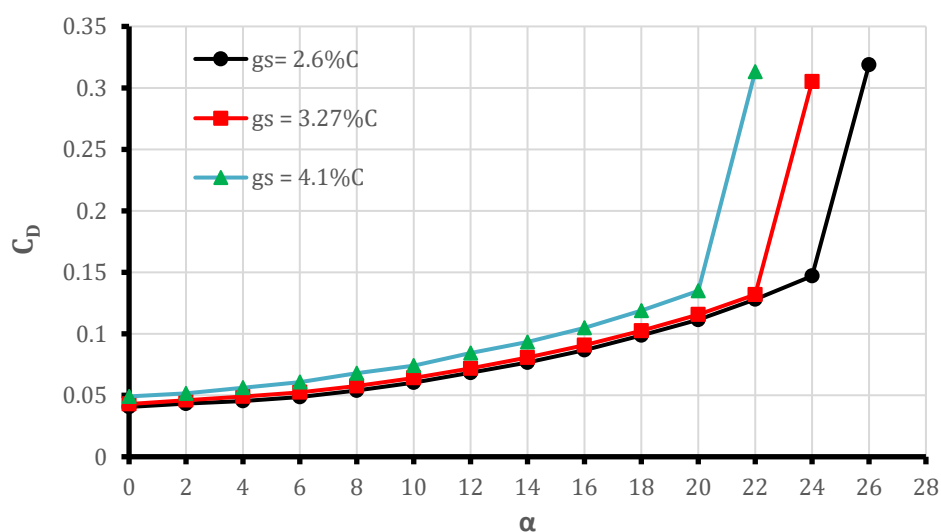Figure 7. Lift coefficient for different gaps of slats.

Figure 8. Drag coefficient for different gaps of the slat.

iii. Effect of overlapping

Figure 9 shows the C_l value for each angle of attack of the airfoil with various overlaps. It can be observed that the negative overlap increases lift generation, especially at lower speeds and higher angles of attack.   This configuration can help maintain attached airflow over a wider range of angles, delaying stall and improving high-lift performance.   The overlap of 0% C is a neutral configuration that has no overlap, creating a more straightforward airflow path without the benefits of slat interaction. With this configuration, the stall angle is slightly reduced compared to configurations with negative overlap, potentially increasing stall risk at higher angles of attack. At last, the positive overlap may cause significant airflow separation at the leading edge, leading to a decrease in lift and earlier stall onset as shown below. Figure 10 shows the results obtained for the drag coefficient when changing the overlap on the airfoil at different angles of attack. It was observed that the drag is slightly increased with the decrease of overlap due to the additional surface area and complexity of the flow.
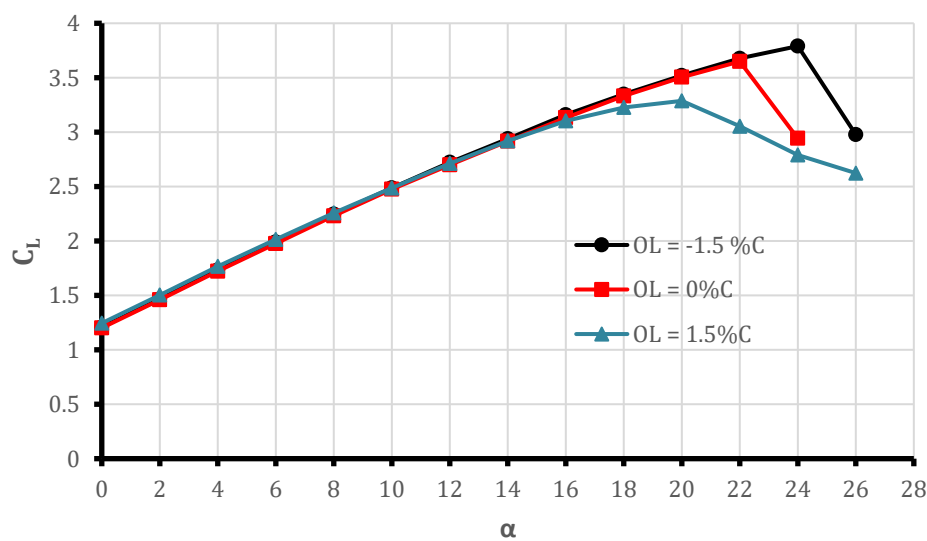

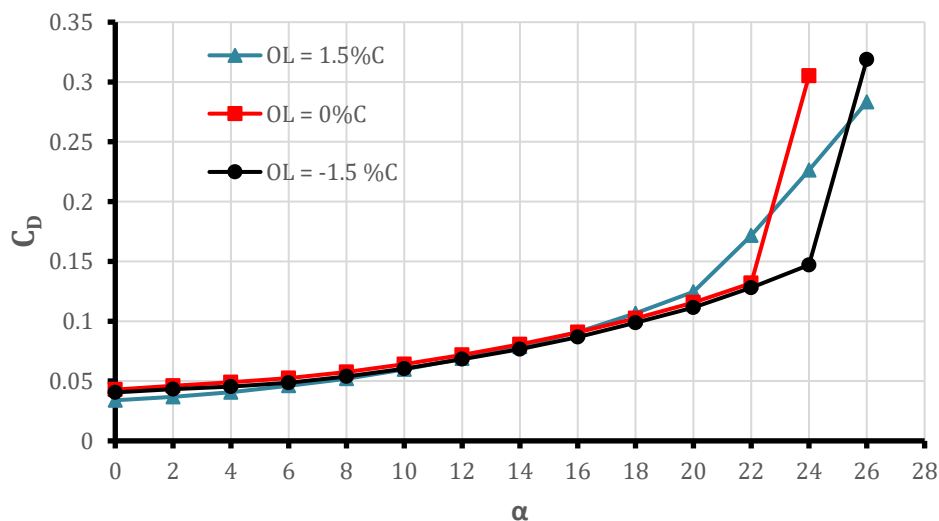Figure 9. Lift coefficient for different overlapping of slats.

Figure 10. Drag coefficient for different overlapping of slat.

4.2   Trailing Edge Flap Effects

For this portion of the study, the slat position was fixed at the optimum location as determined from the previous section, i.e. the slat deflected 30° with x - axis located at a gap of 2.6%C and an overlapping of -1.5% C.

i.   Effect of deflection angle

In the case of constant flap gaps and overlaps and varying flap deflections, it can be observed from Figure 11 that as the flap deflections increased from 10 - 35°, the lift increases significantly. The increase in lift can be attributed to the fact that increasing flap deflection leads to higher camber on the multi-element system, causing higher flow curvature, thereby increasing lift at maximum lift (Cl_{max}) at stall angles. Once the flap angle is set to very high deflections (δf = 35°), the flow on the flap is fully separated, resulting in a lower curve slope and lowering (Cl_{max}). Figure 12 shows the variation of the drag coefficient for different flap deflection angles, where there was an increase in drag as the deflection angles increased.
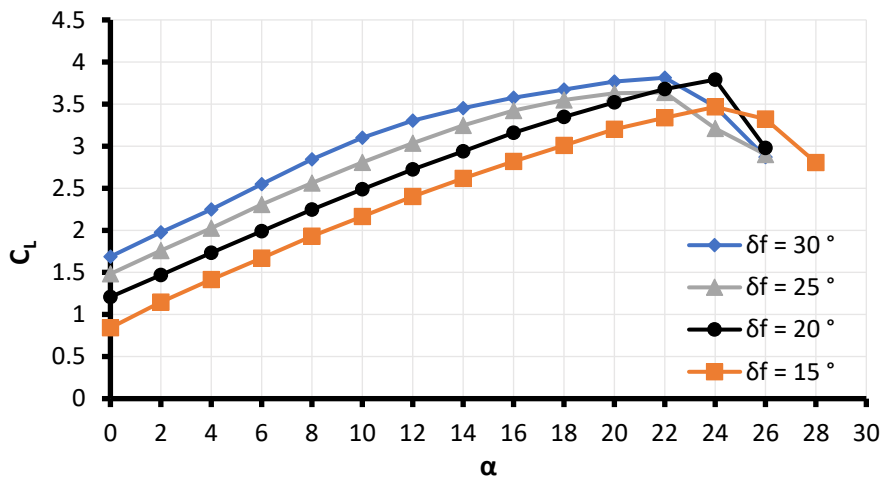

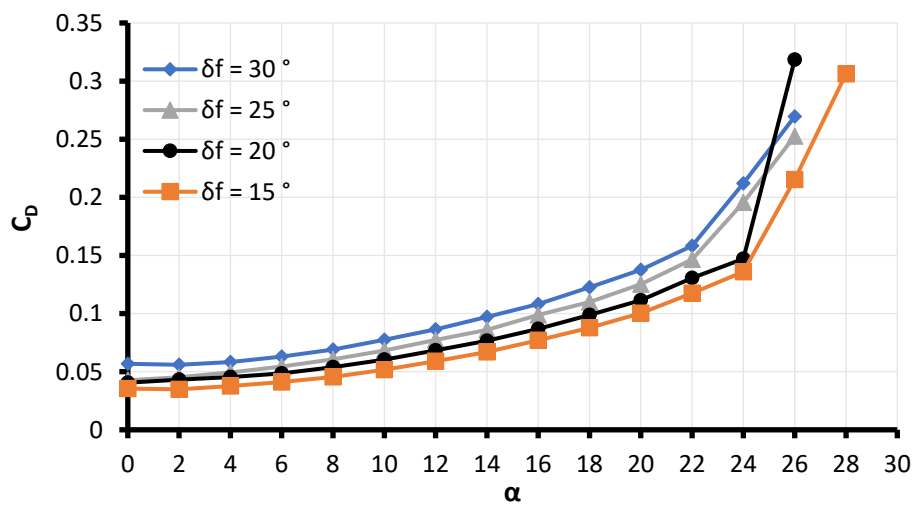Figure 11. Lift coefficient for different deflection angles of the flap.

Figure 12. Drag coefficient for different deflection angles of the flap.

ii. Effect of gap

In the case of constant flap deflections angles and overlapping and varying flap gaps, The flap deflection was fixed at 20 °, it can be observed from Figures (13) and (14), that the smaller gap values (1.3%C) generally enhance aerodynamic performance, while larger gaps (5.7%C) can lead to significant reductions in lift and increases in drag. However, the curves of all the cases are similar at low angles of attack, while at higher angles of attack, the effect of the gap is more pronounced.
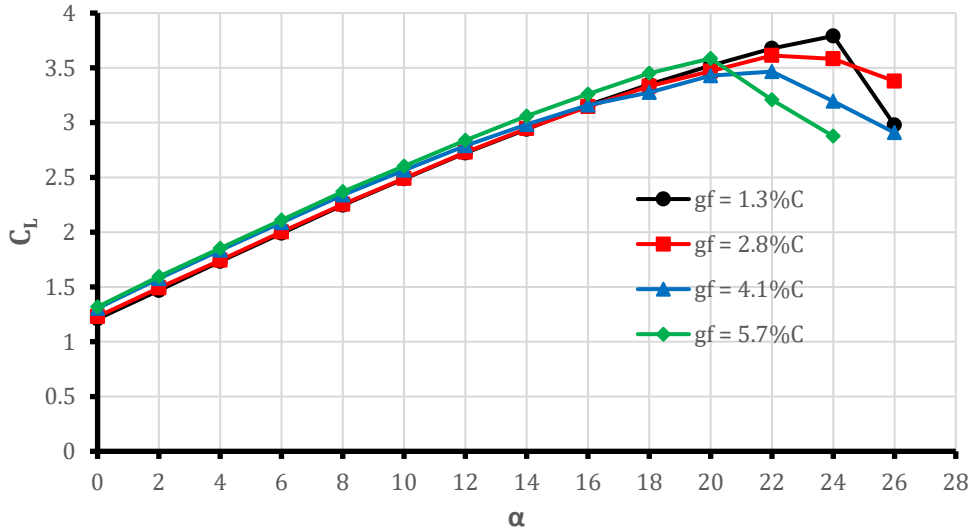
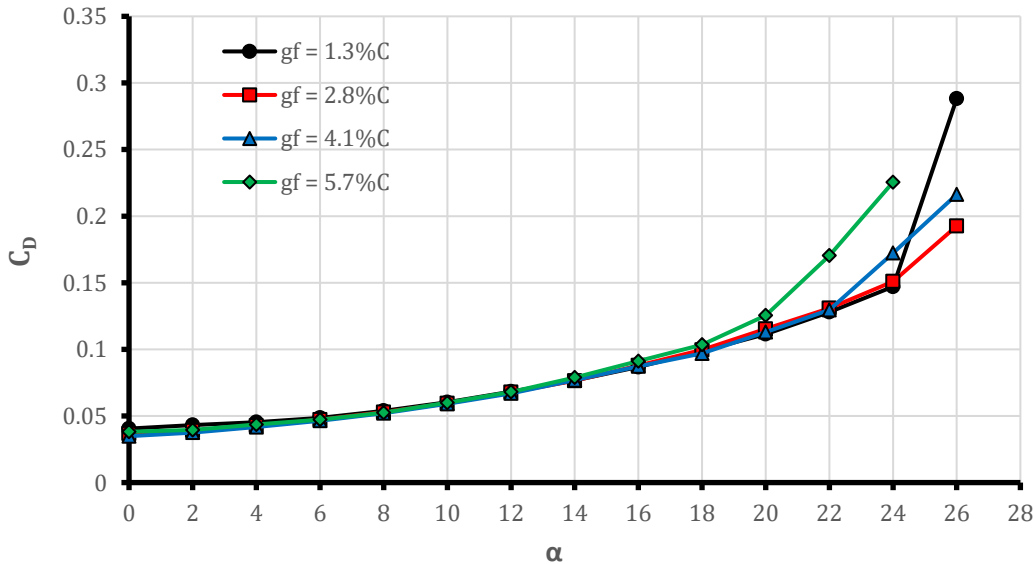Figure 13.   Lift coefficient for different gaps of the flap.

Figure 14. Drag coefficient for different gaps of the flap.

iii. Effect of overlapping

The effect of overlap on flap performance was investigated, keeping the gap at 1.3%C and the deflection angle was fixed at 20 °. It can be observed that when the overlapping increased to - 2.5%C, the results showed that the lift is significantly reduced and the drag increased, as shown in Figure 15 and Figure 16, respectively. This is due to the separation that takes place on the flap, which can have a global effect on the flow over the upper surfaces of the entire high-lift system.
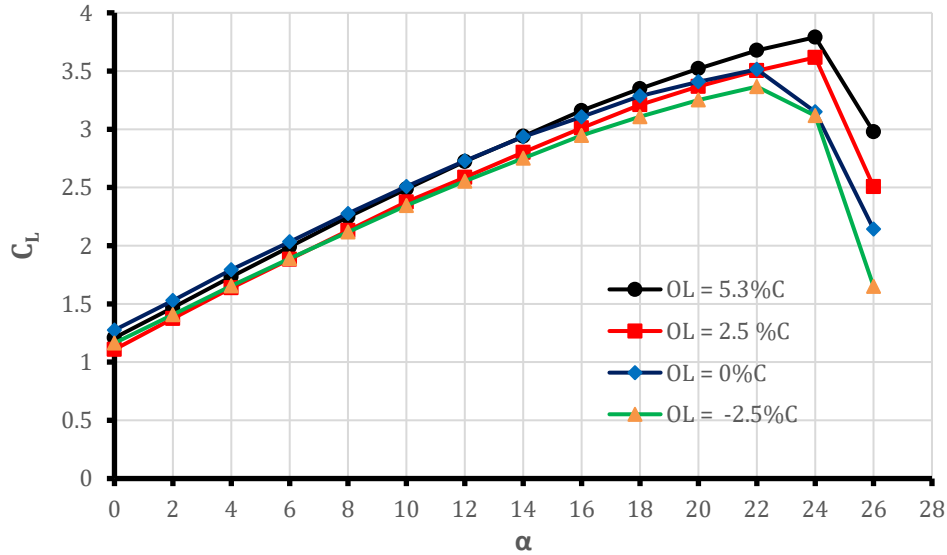

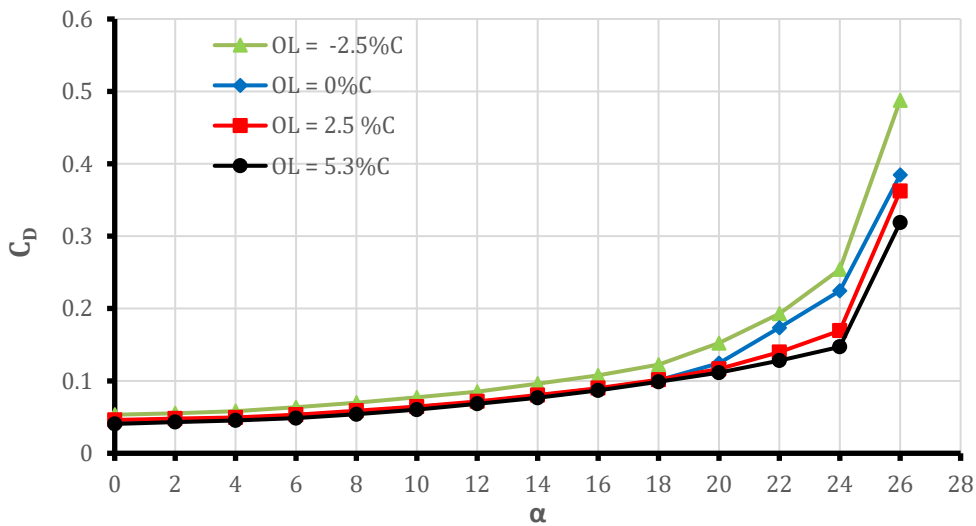Figure 14.   Lift coefficient for different overlappings of the flap.

Figure 15. Drag coefficient for different overlapping of the flap.

4.3 Flow Visualization

At an optimum slat position as determined in the study, and at determined flap rigging, the flow was visualized to generate the velocity and pressure contours as well as streamlines, to show the flow behaviour over a multi-element airfoil at different angles of flap deflection. Three different flap deflections, that is, $\delta_f = 15°$, $25°$ and $35°$ were present at different angles of attack. Iso-contours of pressure and velocity are shown in Figure 16 and 17, respectively.

At each given deflection angle, the contours showed that at low angles of attack (0° to 5°), the airfoil operates efficiently with attached flow, generating moderate lift and maintaining smooth velocity and pressure distributions. As the angle of attack increases up to 10°, a significant lift is generated, accompanied by enhanced suction on the upper surface and increased flow acceleration, though the risk of flow separation begins to emerge. At higher angles beyond 10°, the airfoil approaches stall conditions, exhibiting pronounced flow separation, irregular pressure contours, and a dramatic decrease in lift effectiveness. Also, these contours give an idea of the expanding separated region with recirculation above the flap by increased flap deflection. It can be observed that at a deflection angle of 15° and 25° for low angles of attack (< 20°), the flow on the flap is fully attached until the flow separates on the main airfoil element at higher angles.

This can also be seen by visualizing the flow streamlines as shown in Figure 18. Once the flap angle is set to $\delta_f = 35°$ or higher values, the contours show, the flow on the flap is fully separated, resulting in a lower lift while drag increased.
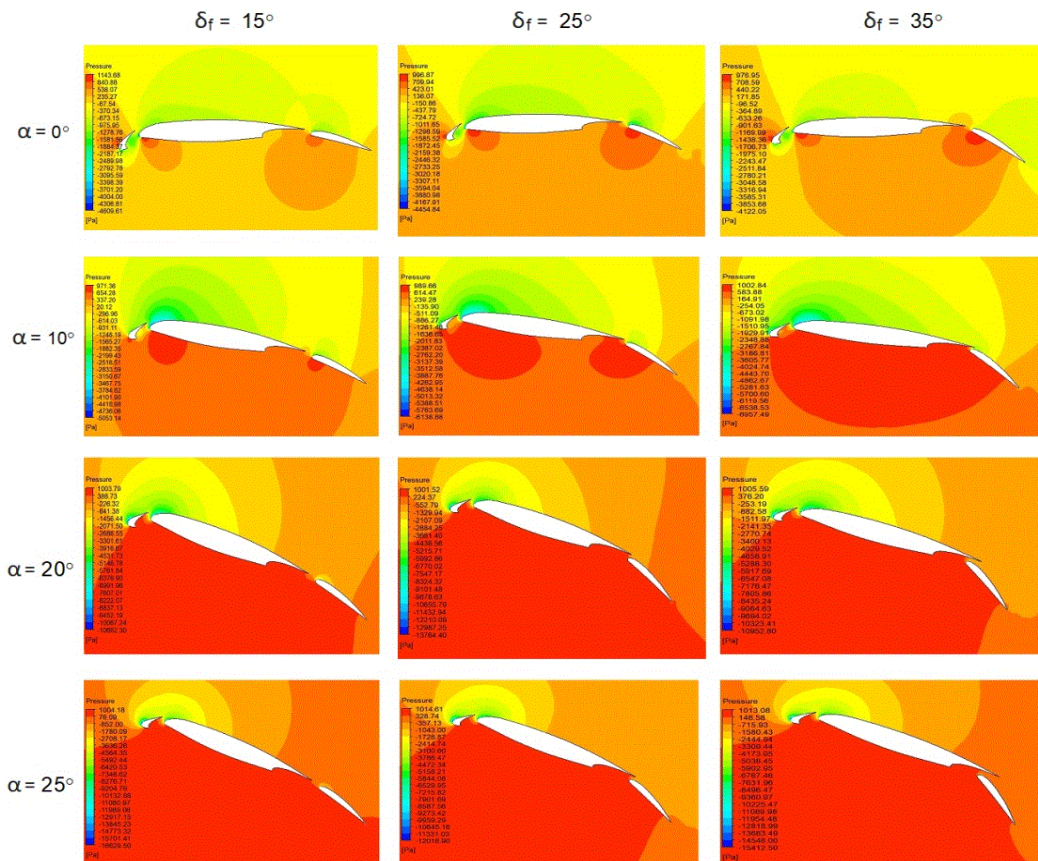

Figure 16. Pressure contours at optimum flap location and different deflection angles.
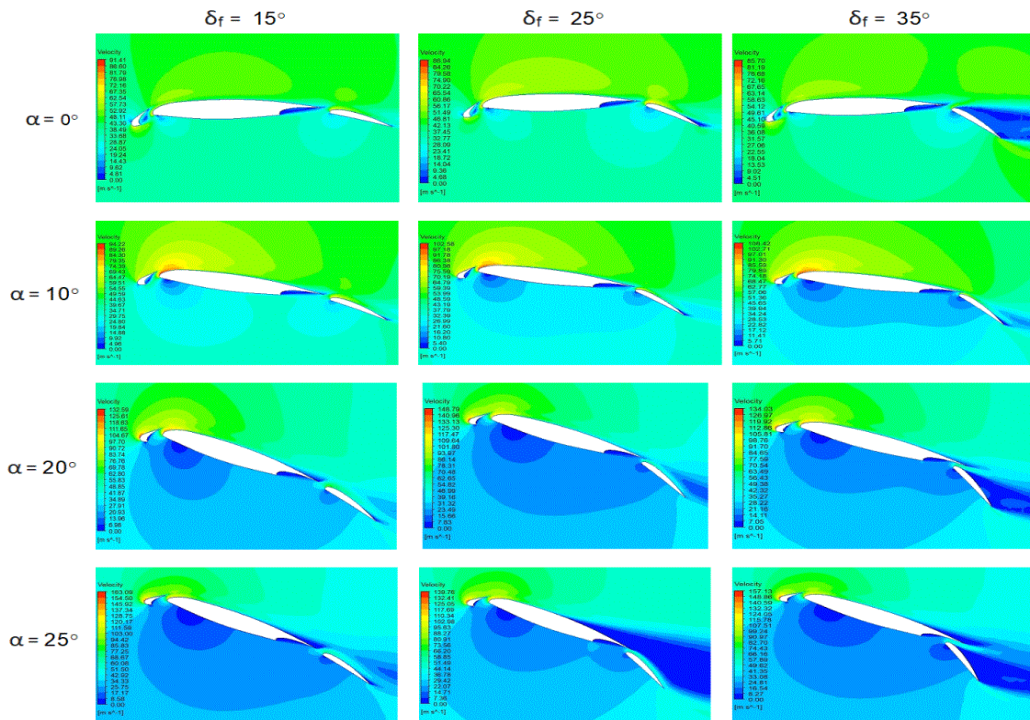
Figure 17.   Velocity contours   at optimum flap location and different deflection angles.
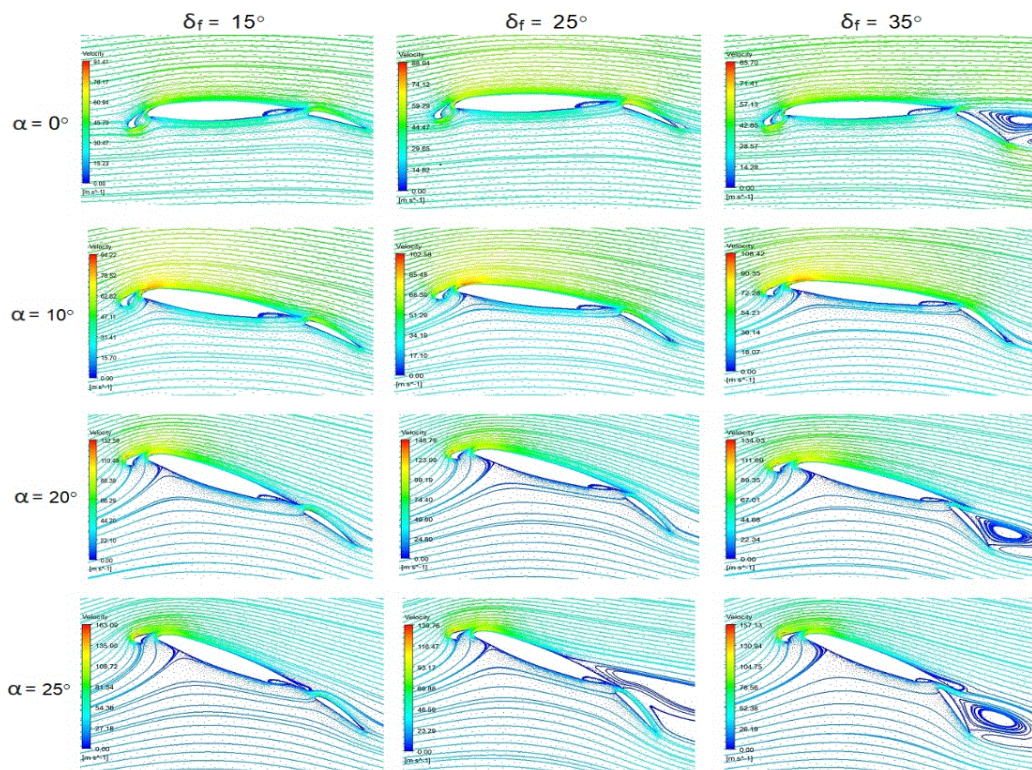

Figure 18. Streamlines at optimum flap location and different deflection angles.

5. Conclusions

The airfoil NHLP with leading edge slat, main element and training edge flap was studied. The effect of varying locations, that is, the deflection angles, gaps and overlaps on the aerodynamic characteristics was investigated. The results reveal that the multi-element airfoils enhance lift performance compared to single-element airfoils, especially during critical phases like take-off and landing. Several salient conclusions can be drawn from this work, including:

1. At a fixed flap location, lowering slat deflection angles, gap and negative overlapping improve Cl$_{max}$ and delay stall angles.

2. It was found that from the slats tested, the 12.5%C, chord length ratio with a 2.6% gap, -1.5% overlap, and 30° flap deflection was the one with the most favourable performance, generating a Cl_{max} of 3.79 and Cd of 0.147.

3. Flap deflection angle was the most influential parameter, where the lift and drag increased significantly as the angles increased, but for high deflection angles more than 30°, the lift dropped, but the drag continuously increased.

4. It was found that the 33%C chord length ratio flap with a 1.3% gap, 5.3% overlap and 30° flap deflection was the one with the most favorable performance, generating a Cl_{max} of 3.81 and Cd of 0.158.

REFERENCES

[1] Arra A, Anekar N, Nimbalkar S., Aerodynamic effects of Leading Edge (LE) slats and slotted Trailing Edge (TE) flaps on NACA-2412 airfoil in prospect of optimization, *Mater Today: Proc*. 2021, vol. 44, pp.:587-595.

[2] Smith, A. M. O., High-Lift Aerodynamics, *Journal of Aircraft*, 1975. vol. 12, pp: 501-530.

[3] Unni, T.A., Experimental investigation on the effect of wall functions on different configurations of a multi a multi-element wing, *Proceedings of the 23rd AIAA Computational Fluid Dynamics Conference*, 2017.

[4] Jawahar, H. K., Azarpyevand, M., & Carlos, R. S., Experimental investigation of flow around three element high lift airfoil with Morphing Fillers, *23rd AIAA/ CEAS Aero-Acoustics Conference.* Denver, Colorado, 2017.

[5] Wang, J., Wang, J., Kim, K. C., Wake/shear layer interaction for low-Reynolds-number flow over multi-element airfoil, *Experiments in Fluids*, 2018, 60 (1).

[6] Gao, J., Li, X., Lin, D., Numerical Simulation of the Noise from the 30P30N High lift Airfoil with Spectral Difference Method. *23rd AIAA/CEAS Aeroacoustics Conference*. 2018.

[7] Jin, Y.; Liao, F.; and Cai, J., Numerical simulation of 30p30n multi-element airfoil using delayed detached-eddy simulation, *Proceedings of the AIAA Aviation 2020 Forum*, June 15-19, 2020

[8] Xiao, M.; Zhang, Y.; and Zhou, F., Numerical investigation of the unsteady flow past an iced multi-element airfoil, *AIAA Journal*, 2020, vol. 58, No. 9, pp.: 3848-3862.

[9] Shahrokhi, S. S., Rahni, M., T., and Akbari, P., Aerodynamic design of a double slotted morphed flap airfoil – a numerical study, *Frontiers in Mechanical Engineering*, 2024.

[10] Huang, S., Qiu, H., and Wang, Y., Numerical study of aerodynamic performance of airfoil with variable curvature split flap, *J. of Applied F. Mechanics*, 2023, vol. 16, No. 6, pp: 1108-1118.

[11] Hariyadi, S. P., Junoitoyo, B., Pambudiyatno, N., S., Widodo, W. A., Aerodynamic characteristics of fluid flow on multiple element wing airfoil NACA43018 with leading edge slat and plain flap, *J. of Engg. Sc. and Technology ICIST*2022, 2023, vol. 18, No. 1, pp.: 36 – 50.

[12] Khormi, H., and Alfifi, S., Multi-element Airfoil Analysis for NACA 0012 Using Computational Fluid Dynamic, *AIAA SciTech Forum* 2022.

[13] Bhargava, V. , Dwivedi, Y. D., Rao, P. M. V., Analysis of multi-element airfoil configurations: a numerical approach, *MOJ Applied Bionics and Biomechanics*, 2017, vol. 2, pp.: 83-88.

[14] Elsafty, K. A. I., Elsherif1, A. M. E., Ibrahim, A. A., Mohamed, O. S., Elbaz, A. M. R., Investigating the Performance of a Novel Multi-Element Airfoil Concept Using Numerical Analysis, *J. of Advanced Research in F. Mechanics and Thermal Sc.*, 2022, Issue 2, pp: 126-145.

[15] Sharma P., Kumar P., Singh R. K., Optimum Slat and Flap Configuration for Maximizing Lift on NACA-4412 Airfoil at Various Angle of Attack, Using XFOIL at a Reynolds Number of 1 Million, *J. of Appl. Mech. Eng.*, 2023, vol. 12 :485.

[16] Fonseca, W. D. P.,   Reis, M. W. F., Dias, P. F. L., and   Filho, M. L. S., CFD Analysis of airfoils with flaps for low Reynolds Numbers, *REPA Journal*, 2019, vol. 4, No. 4, pp: 93-101.

[17] Hami, K.,   Turbulence Modeling a Review for Different Used Methods, *International Journal of Heat and Technology*, 2021, vol. 39, No. 1, pp: 227 – 234.

[18] Menter, F. R., Two-Equation Eddy-Viscosity Turbulence Models for Engineering Applications, *AIAA Journal,* 1994, vol. 32, No. 8, pp. 1598–1605.

[19] Information on the k-ω SST model is available at:
http://turbmodels.larc.nasa.gov/sst.html. accessed on 10/03/2024.

[20] Moir, I. R. M., Measurements on a Two-Dimensional Aerofoil With High-Lift Devices, *A Selection of Experimental Test Cases for the Validation of CFD Codes – AGARD AR-303*, 1994, vol. 2, pp. A2-1–A2-12.

[21] Lei, Z., Murayama, M., Takenaka, K., Yamamoto, K., CFD validation for high-lift devices: Two-element airfoil. *Trans. Japan Soc. Aero. Space Sci.*, 2006, vol. 49(163), pp: 31–39.

[22] Anderson, J. D. Jr, FUNDAMENTALS OF AERODYNAMICS, sixth edition, McGraw-Hill International Editions, New York, USA, 2017, pp. 3–98.

[23] Suvanjumrat C., Comparison of Turbulence Models for Flow Past NACA0015 Airfoil Using OpenFOAM, *Engineering Journal*, 2017, Volume 21 Issue 3, pp: 208-221.

[24] ANSYS Fluent Theory Guide 2019, ANSYS, Inc.: Canonsburg, PA, USA.

[25] Sereez, M. and Zaffar, U., Dynamic Stall on High-Lift Airfoil 30P30N in Ground Proximity, *Open Journal of Fluid Dynamics*, 2021, vol. 11, pp: 135-152.